

Simulation of matrix acidiza- tion with self- diverting acid systems

J.R. Guerrero



Simulation of matrix acidization with self-diverting acid systems

by

J.R. Guerrero

to obtain the degree of Master of Science
at the Delft University of Technology,
to be defended publicly on Tuesday December 23, 2020 at 10:00.

Student number: 4285891
Project duration: January 1, 2019 – December 23, 2020
Thesis committee: Prof. Dr. P.L.J. Zitha, TU Delft, supervisor
Dr. D. V. Voskov, TU Delft, supervisor
Dr. D. S. Draganov, TU Delft, supervisor

An electronic version of this thesis is available at <http://repository.tudelft.nl/>.

Preface

Before you lies the MSc thesis 'Simulation of matrix acidization with self-diverting acid systems', which describes my graduate research project to develop a simulator for simulating matrix acidization with self-diverting acid systems. This work has been done within the DARTS-framework developed by D.V. Voskov at Delft University of Technology. The report has been written to fulfill the graduation requirements of the Applied Earth Sciences - Petroleum Engineering specialization, at Delft University of Technology. I was engaged in researching and writing this thesis from January 2019 till December 2020.

The project was undertaken at the request of Sidney van den Berg, Chief Operating Officer at Symoil Group at the time of writing. My research question was formulated together with my supervisor Pacelli Zitha, and the simulation approach has been supervised by Dennis Voskov.

I would like to thank my two main supervisors for their guidance and support during this process. I also wish to thank Deyan Draganov for taking the time to read make thesis and attend the colloquium. Lastly I want to thank PhD students Xiacong Liu and Stephan de Hoop for the daily supervision, without whose cooperation I would not have been able to conduct this analysis.

I hope you will enjoy reading this thesis.

Joey Guerrero
Delft, December 16, 2020

Contents

List of Symbols	1
List of Figures	3
List of Tables	1
1 Introduction	3
1.1 Introduction	3
1.2 Self-diverting acid blends	4
2 Physics	5
2.1 Governing equations	5
2.1.1 Conservation of species	5
2.1.2 Single-phase flow.	6
2.2 Visco-elastic surfactant.	7
2.2.1 Rheological model for apparent viscosity	8
2.2.2 Parameter range	8
2.2.3 Effective viscosity.	10
2.2.4 Complete rheological model for apparent viscosity	11
2.2.5 Apparent viscosity	11
2.3 Porescale parameters	11
2.3.1 Porosity	11
2.3.2 Permeability.	12
2.3.3 Pore structure.	12
2.4 Reaction rate	12
2.5 Mass-transfer coefficient	14
3 Numerical model	17
3.1 Operator-Based Linearization	17
3.2 Viscosity treatment	17
3.2.1 Reaction rate	18
3.2.2 Molar composition to weight percent conversion	18
3.3 Operators	19
4 Results	21
4.1 Results and discussion 1D.	21
4.2 Initial results 2D.	22
4.3 Results full-complexity 2D model	23
4.4 Results simplified 2D model	25
4.4.1 Numerical instabilities	26
4.5 Sensitivity analysis	26
4.6 Conclusion and recommendations.	32
Bibliography	33

List of Symbols

- ϕ : porosity
- t : time [d]
- ρ_f : fluid density [kg/m^3]
- ρ_s : solid density [kg/m^3]
- v_{ck} : stoichiometric coefficient of kinetic reaction k
- v_{cq} : stoichiometric coefficient of equilibrium reaction q
- r_k : reaction rate of kinetic reaction k
- r_q : reaction rate of equilibrium reaction q
- s_f : fluid saturation
- s_s : solid saturation
- x_{cf} : mole fraction of component c in fluid phase
- x_{cs} : mole fraction of component c in solid phase
- \underline{u}_f : fluid velocity [m/d]
- \underline{D} : diffusivity coefficient
- m_c : mass of component c
- $wt\%_c$: weight percentage of component c
- n_c : number of moles of component c
- l_c : flux of component c
- MW_i : molecular weight of component c
- k_c : Mass-transfer coefficient [m/s]
- k_B : Boltzmann constant [$m^2 kg s^{-2} K^{-1}$]
- T : Temperature [K]
- $r_{particle}$: radius of diffusing particle [m]
- μ_0 : base viscosity of acid blend [$Pa * s$]
- μ_a : apparent viscosity of acid blend [$Pa * s$]
- μ_e : effective viscosity of acid blend [$Pa * s$]
- r_p : pore radius [m]
- \underline{u} : fluid velocity [m/s]
- C : concentration [mass percent]
- C_m : concentration at which viscosity reaches maximum [mass percent]
- a : scaling parameter for acid model
- b : scaling parameter for acid model
- c : scaling parameter for acid model
- $W1$: scaling parameter for acid model
- $W2$: scaling parameter for acid model
- $W3$: scaling parameter for acid model

List of Figures

1.1	Visco-elastic diverting acid. [9]	4
2.1	An example of a structural formula of a zwitterion.	7
2.2	Visco-elastic mechanism of diverting acid	7
2.3	acid composition vs multiplication factor	8
2.4	pH vs multiplication factor	9
2.5	VES vs multiplication factor	9
2.6	Ca^{2+} vs multiplication factor	10
2.7	Acid propagation from the pore to the solid-fluid interface	13
4.1	1D non-reactive simulation results.	21
4.2	1D reactive simulation results.	22
4.3	2D simulation results for homogeneous reservoir with constant viscosity and constant reaction rate.	22
4.4	2D simulation results for heterogeneous reservoir with constant viscosity and constant reaction rate.	23
4.5	2D simulation results for viscosity variations. First row is results for constant viscosity. Second row is results for state-dependent viscosity. Third row is results for state- and shear-dependent viscosity.	23
4.6	2D simulation results for full viscosity model, as described in Physics section.	24
4.7	2D flow lines results for full viscosity model, as described in Physics section.	24
4.8	2D simulation results for simplified viscosity model for pressure, acid and surfactant compositions, viscosity, porosity and permeability	25
4.9	2D simulation flow lines for simplified viscosity model.	25
4.10	Sensitivity of multiplication factor to acid and VES composition.	27
4.11	plot results for $k_{upperlayer} = 400mD$, run time = 1000d, dt = 5d, $\mu_{max} = 10500cP$	27
4.12	flowlines for $k_{upperlayer} = 400mD$, run time = 1000d, dt = 5d, $\mu_{max} = 10500cP$	28
4.13	plot results for $k_{upperlayer} = 20000mD$, run time = 10d, dt = 0.2d, $\mu_{max} = 10500cP$	28
4.14	flowlines for $k_{upperlayer} = 20000mD$, run time = 10d, dt = 0.2d, $\mu_{max} = 10500cP$	29
4.15	plot results for $k_{upperlayer} = 4000mD$, run time = 1.7d, dt = 0.2d, $\mu_{max} = 350cP$	29
4.16	flowlines for $k_{upperlayer} = 4000mD$, run time = 1.7d, dt = 0.2d, $\mu_{max} = 350cP$	30
4.17	plot results for $k_{upperlayer} = 4000mD$, run time = 1500d, dt = 5d, $\mu_{max} = 21000cP$	30
4.18	flowlines for $k_{upperlayer} = 4000mD$, run time = 1500d, dt = 5d, $\mu_{max} = 21000cP$	31

List of Tables

4.1	1D 6-component simulation injection and initial conditions	22
4.2	Simulation parameters for results and sensitivity analysis	31

Introduction

1.1. Introduction

Oil and gas reservoirs are found in the subsurface in various types of rock formations, which all have different flow properties. Properties vary between different geological formations, but also within each geological formation variations are found. These variations (heterogeneity) are caused by changes in the depositional environment over geological time, causing the mineral composition of the rock mass to vary in space. This difference in composition causes flow properties to vary over the reservoir which complicates the recovery of hydrocarbons because fluids can flow easily in some parts of the reservoir, while in other parts there could be no substantial flow. One of these issues is partial depletion of a reservoir. A reservoir can roughly be subdivided into low and high permeable zones. Because the high permeable zones allow for easier flow of hydrocarbons, these will often be depleted first, leaving the low permeable zones saturated with oil. Another problem is that high pressure differences between the wellbore and the reservoir cause fines to migrate towards the wellbore, settling in the pore space and obscuring flow paths near the well bore. This causes local zones of decreased porosity and permeability near the well. As all flow converges in this region, obstructions in flow-paths in the near-wellbore region have more impact than they would have further away from the wellbore. The resulting decrease in porosity reduces effective permeability, which lowers the flow rate and thus the productivity index of the well. [12] This is also known as formation damage. In carbonate reservoirs this can also occur due to mineral deposition of soluble minerals ($CaCO_3$ among others).

A technique frequently employed in carbonate reservoirs to increase the flow of fluids in these low-permeability zones is acid stimulation. This is used both in hydrocarbon and geothermal reservoirs. Matrix rock is dissolved during this process by injection of an acid blend which creates new wormholes through which fluids can flow. [11] The problem with this however, is that injected fluid tends to enter the parts of the reservoir that have high permeability and enlarge the permeability in these zones, while the aim is to target low-permeability zones. One way to improve stimulation of low-permeability zones is by using self-diverting acid blends, which contain a surfactant that increases the viscosity of the fluid when the pH drops as a result of acid being spent in reaction. [6] Acid will flow into high permeability regions first, where the viscosity will increase due to the spending of acid. This increase in viscosity will block the flow of fluids so that the acid gets diverted into low-permeability zones.

The goal of this thesis is to develop a reservoir simulator to make initial analysis on matrix acidizing with self-diverting acid systems in the region surrounding the wellbore. Through simulation we hope to find answers to the following questions:

- Until what permeability difference is using self-diverting acids still effective, and at what point is it necessary to switch to mechanical diversion methods?
- If wormholes exist from a previous acidizing job, will self-diverting acid still be successful at diverting flow and creating wormholes in low-permeability zones?

The simulations are made in the Delft Advanced Research Terra Simulator (DARTS) framework developed at TU Delft.

1.2. Self-diverting acid blends

In heterogeneous reservoirs with a large variety of pore structures or permeability, acid preferably enters the region with the highest permeability, leaving the low-permeability zone untreated after injection. As a result, the magnitude of permeability variance between layers continues to increase. [7] This is an unwanted result because stimulation of the low-permeability zones yields the biggest increase in oil recovery. Preferably new flow paths are to be created in the low permeability region, to maximize stimulation of hydrocarbon flow in these zones, and maximize zonal coverage. To achieve this, effective fluid placement is needed to successfully treat heterogeneous reservoirs. Injection of self-diverting acid achieves this by diversion of flow from the high permeability zone to the low permeability zone.

Flow diversion methods can be divided into either mechanical or chemical techniques. Mechanical diversion methods mainly include coiled tubing-conveyed tools with mechanical packers that isolate an interval and direct fluid into low-permeability layers, or by using ball-sealers that seal off the perforation of a high-permeability. [1] Chemical diversion methods can be classified into foam acid, in-situ cross-linked acid and self-diverting acid [7]. This thesis focuses on simulating acid stimulation with self-diverting acid blends. A self-diverting acid blend is a mixture that contains surfactants which increase the fluids viscosity, based on the concentration of acid, surfactant and calcium ions. When the mixture gets injected, the acid (typically hydrochloric acid, HCl) reacts with the rock matrix (typically calcium carbonate, $CaCO_3$), which reduces the presence of H_3O^+ ions and increases the presence of Ca^{2+} ions. Injected acid blend will follow the path of least resistance and flow into the high permeability zone first, where this reaction will initially occur. Upon spending of the acid in the high-permeability zone, the viscosity steeply increases due to the visco-elastic properties of the surfactant, forcing the acid to find a different path through the reservoir by entering the low-permeability region and thus effectively stimulating the target region. The exact mechanism that causes this will be discussed in the physics section. Figure 1.1 shows a photo of visco-elastic diverting acid [9].



Figure 1.1: Visco-elastic diverting acid. [9]

2

Physics

This chapter describes the physics that will be implemented into the simulator. The first section describes the governing equations needed for the simulation. The second section describes the viscosity-varying mechanism and the viscosity model. The mechanism of visco-elastic acid blends is explained, after which the individual parameters and their theoretical sensitivity will be evaluated. Visco-elastic surfactant containing fluids behaves like a non-Newtonian shear-thinning fluid, so a shear model will be introduced. The individual parameters and shear model will be combined in section 2.2.4 to form the full rheological model for apparent viscosity to be implemented. Next, the porosity and permeability will be described. In the last four sections, the reaction rate and the parameters needed to determine this, will be discussed.

2.1. Governing equations

2.1.1. Conservation of species

We start with the most general formulation of the mass balance for component c as described by Voskov [10]:

$$\frac{\partial n_c}{\partial t} + l_c + q_c = \sum_{k=1}^{k=N_k} v_{ck} r_k + \sum_{q=1}^{q=N_q} v_{cq} r_q \quad (2.1)$$

Where the first term represents accumulation, the second term represents flux which consists of convective and diffusive flux, the third term represents the source term, fourth term are kinetic reactions and the fifth term are equilibrium reactions. N_k and N_q are the number of kinetic and equilibrium reactions that occur, respectively.

n_c represents the overall mass of component c :

$$n_c = \sum_{f=1}^{f=N_f} (\phi \rho_f s_f x_{cf}) + \rho_s (1 - \phi) x_{cs} \quad (2.2)$$

Where N_f denotes the total number of fluid phases, and thus the first term describes the total mass of component c in all the fluid phases, the second term describes the mass of component c in solid phase. l_c represents the flux of component c in the fluid phases:

$$l_c = \nabla \cdot \sum_{f=1}^{l=N_f} (\rho_f x_{cf} \underline{u}_f - \rho_f \phi s_f D \nabla x_{cf}) \quad (2.3)$$

The source term q_c reads:

$$q_c = \sum_{f=1}^{l=N_f} (\rho_f x_{cf} q_f) \quad (2.4)$$

2.1.2. Single-phase flow

Simulating two-phase flow makes the simulation substantially more complex. As diversion of fluid flow caused by self-diverting acids is predominantly based on fluid phase properties and chemical reaction rate, it has been decided to simplify the physics by assuming full dissolving of gaseous phase minerals components, leading to single-phase flow. Diffusion on a reservoir scale will also be neglected. The mass balance equation (eq 2.1), will be simplified for single-phase flow without diffusion.

The expression for overall mass of the c^{th} component (eq 2.2) for single-flow is given for liquid components by:

$$n_c = \phi \rho_f S_f x_{c,f} \quad (2.5)$$

And for solid phase components by:

$$n_c = \rho_s (1 - \phi) x_{c,s} \quad (2.6)$$

If diffusion is neglected, equation 2.3 for single-phase flow reads:

$$l_c = \nabla \rho_f x_c \underline{u} \quad (2.7)$$

In single-phase flow, the source term becomes:

$$q_c = \rho_f x_c q \quad (2.8)$$

The general form of the mass balance for the c^{th} fluid component in single-phase flow without diffusion, considering only one kinetic reaction, now reads:

$$\frac{\partial(\phi \rho_f x_c)}{\partial t} + \nabla(\rho_f x_c \underline{u}) + \rho_f x_c q = v_c r_k \quad (2.9)$$

The solid species is dissolved into the liquid phase, such that the solid composition decay is [5]:

$$\frac{\partial x_5}{\partial t} = \sum_{k=1}^{k=N_k} v_{5,k} r_k \quad (2.10)$$

Where x_5 is the solid composition Or if only one reaction is considered:

$$\frac{\partial x_5}{\partial t} = v_5 r \quad (2.11)$$

Substituting these into equation 2.1, gives the following equation for mass balance of component c in fluid phase:

$$\frac{\partial}{\partial t} \phi(x_c \rho_f S) + \nabla(x_c \rho_f \underline{u}) + x_c \rho_f q = v_c r \quad (2.12)$$

2.2. Visco-elastic surfactant

Adding visco-elastic surfactant to the acid blend allows for the viscosity to vary depending on the mixture's chemical composition. Zwitterionic surfactants are the most commonly used surfactant for self-diverting acid blends [4], which are surfactants that can carry different charge characteristics, depending on the pH value. An example of the structural formula of a zwitterion is shown in figure 2.1. This figure shows an example of a molecule that has a zwitterionic isomer. It has an equal number of positive and negative charged groups, so the overall charge of the molecule is neutral. [3]

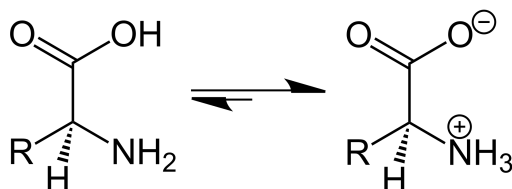


Figure 2.1: An example of a structural formula of a zwitterion.

To explain why at some conditions the molecule is zwitterionic, we first need to define the isoelectric point. The isoelectric point is the pH at which a molecule carries no net electrical charge and is electrically neutral. When the pH value is below the isoelectric point, its anion group ionization is weak and it shows cationic (positively charged) characteristics. So when fresh acid is present the pH is below the isoelectric point and the surfactant will have a positive charge. In this state the molecules are distributed throughout the fluid in the form of monomers, and the fluid viscosity is low. When pH increases past the isoelectric point the ionization degree of anionic groups increases. This means the anionic properties increase, and the cationic properties decrease. When the pH increases enough to reach the isoelectric point the charge will be neutral. The charge effect is weakened, and the surfactant molecules are spherical/ short rod-like micelles. The reaction between the acid and rock matrix causes Ca^{2+} -ions to be present in the solution. The presence of these cations causes cross-linking of the surfactant. The spherical/ rod-like micelles entangle with each-other to form wormlike micelles with a spatial network structure. When this occurs, the viscosity of the system increases sharply and the high-permeability zone is temporarily blocked, causing the subsequent acid to divert and enter the low-permeability zone. When the barrier comes in contact with hydrocarbons, the shape of the micelles will return to spherical geometry and the viscosity will decrease again. This makes well cleanup afterwards easy [4]. This process is shown in figure 2.2

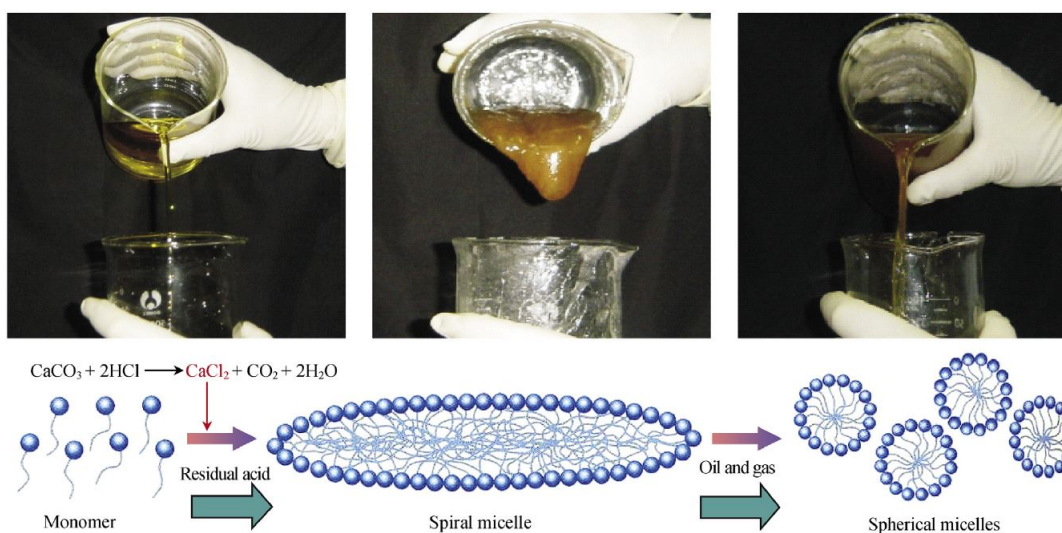


Figure 2.2: Visco-elastic mechanism of diverting acid

2.2.1. Rheological model for apparent viscosity

The viscosity of the fluid is dependent on three variables: Visco-Elastic Surfactant (VES) concentration, pH (acid concentration) and Calcium-ion concentration. When the viscosity changes, the fluid behaves as a shear-thinning fluid, for which a power law equation is used. Isothermal conditions are assumed, so temperature dependency is neglected in this work. The expression for the effective viscosity consists of the fluid's base viscosity plus a maximum viscosity value which is multiplied by three factors between 0 and 1, that each are dependent on one of the compositions. The rheological model used for viscosity of In-Situ self-diverting acid as described by Liu et al [7], is:

$$\mu_a(pH, C_{Ca^{2+}}, C_{VES}) = \mu_0 + \mu_{\max} \times f_1(pH) \times f_2(C_{Ca^{2+}}) \times f_3(C_{VES}) \quad (2.13)$$

where

$$f_1(pH) = \frac{\text{erf}(b \times pH - c) + 1}{W_1} \quad (2.14)$$

$$f_2(C_{Ca^{2+}}) = \exp \left[- \left(\frac{C_{Ca^{2+}} - C_{m,Ca^{2+}}}{W_2} \right)^2 \right] \quad (2.15)$$

$$f_3(C_{VES}) = \exp \left[-0.5 \left(\frac{C_{VES} - C_{m,VES}}{W_3} \right)^2 \right] \quad (2.16)$$

The parameters W_1 , W_2 , W_3 , a , b and c represent scaling parameters, which vary based on the surfactants used. C_m is the concentration (weight percentage) at which apparent viscosity reaches a maximum value. f_1 , f_2 and f_3 are plotted in the next section.

2.2.2. Parameter range

The values for the three functions in the previous section vary between 0 and 1, resulting in the viscosity equation being the base viscosity plus a fraction of the maximum obtainable viscosity, determined by the three multiplication factors that these functions define. The functions are defined such that the real-world physics get approximated, without making the equations too complex. The viscosity spikes when acid is spent (pH increases), in the presence of VES and Ca^{2+} . Figures 2.4 and 2.5, show the viscosity's dependency on acid concentration. The first shows the acid composition on the x-axis, the latter the pH. Figures 2.5 and 2.6 show the influence of VES and Ca^{2+} concentration, respectively.

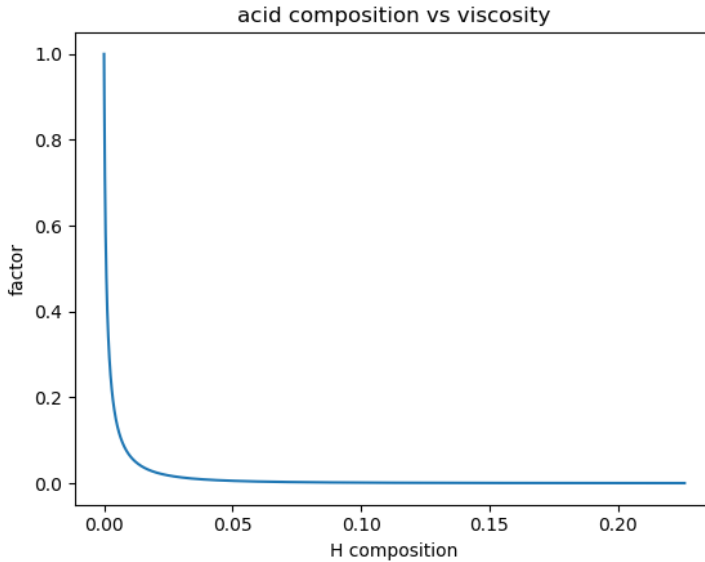


Figure 2.3: acid composition vs multiplication factor

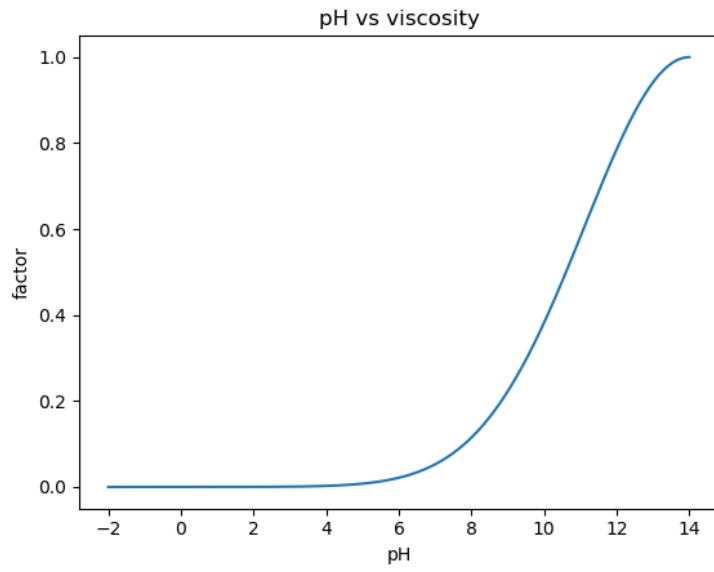


Figure 2.4: pH vs multiplication factor

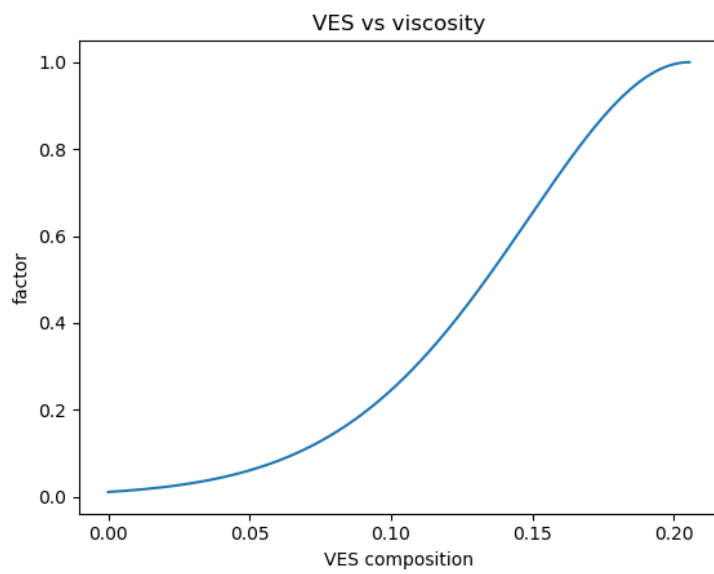


Figure 2.5: VES vs multiplication factor

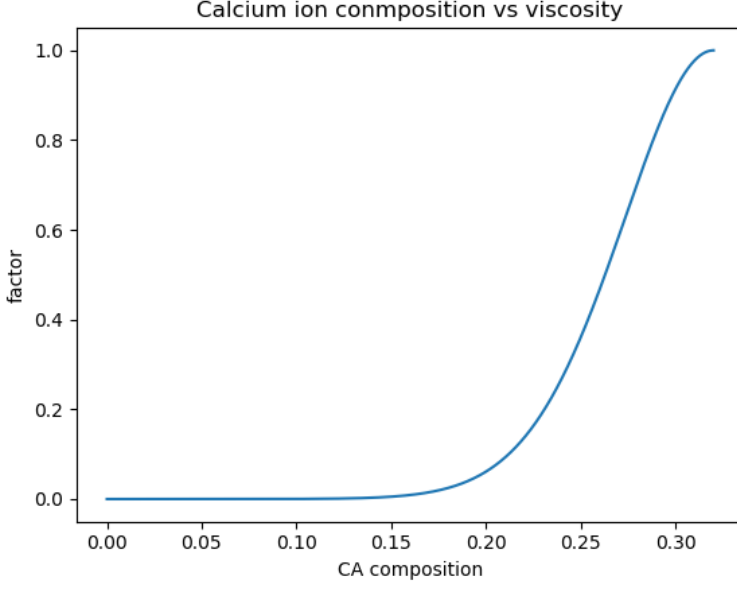


Figure 2.6: Ca^{2+} vs multiplication factor

2.2.3. Effective viscosity

Self-diverting acid is a non-Newtonian fluid and behaves as a shear-thinning fluid. For this reason, an apparent viscosity model is used:

$$\mu_{eff} = \frac{H}{12} \left(9 + \frac{3}{n}\right)^n (150k_d \epsilon)^{(1-n)/2} \quad (2.17)$$

Where H and n are the power-law parameters of consistency factor and power-law index, respectively.

Combining the effects of shear rate and the apparent viscosity model (equation 2.19 and 2.20), the final expression for effective viscosity, based on shear rate, pH, Ca^{2+} and VES concentrations, can be derived:

$$\begin{aligned} \mu_{eff}(\phi, k, pH, Ca^{2+}, VES) &= \frac{\mu_0}{12} \left(9 + \frac{3}{n}\right)^n (150k\phi)^{\frac{1-n}{2}} \\ &\times \left(1 + \frac{\mu_{max}(pH, Ca^{2+}, VES)}{\mu_0} \exp\left(-0.5 \left(\frac{C_{VES} - C_{m,VES}}{W_1}\right)^2\right)\right) \\ &\times \exp\left(-\left(\frac{C_{Ca^{2+}} - C_{m,Ca^{2+}}}{W_2}\right)^2\right) \times \frac{(erf(bpH - c) + 1)}{W_3} \end{aligned} \quad (2.18)$$

2.2.4. Complete rheological model for apparent viscosity

Combining these three equations, the completely rheological model for viscosity of In-Situ self-diverting acid is described as:

$$\begin{aligned} \mu_a(pH, Ca^{2+}, VES) = & \mu_0 + \mu_{\max} \times \exp\left(-0.5 \left(\frac{C_{VES} - C_{m,VES}}{W_1}\right)^2\right) \\ & \times \exp\left(-\left(\frac{C_{Ca^{2+}} - C_{m,Ca^{2+}}}{W_2}\right)^2\right) \times \frac{(erf(bpH - c) + 1)}{W_3} \end{aligned} \quad (2.19)$$

2.2.5. Apparent viscosity

Self-diverting acid is a non-Newtonian fluid and behaves as a shear-thinning fluid. Shear-thinning fluids are fluids whose viscosity decreases under shear strain. For this reason, an apparent viscosity model is used as describes by Ratnakar [8]:

$$\mu_{app} = \frac{H}{12} \left(9 + \frac{3}{n}\right)^n (150k_d \varepsilon)^{(1-n)/2} \quad (2.20)$$

Where H and n are the consistency coefficient and power index, respectively.

Combining the effects of shear rate and the apparent viscosity model (equation 2.19 and 2.20), and substituting the viscosity model into equation 2.20 as H , the final expression for effective viscosity, based on shear rate, pH , Ca^{2+} and VES concentrations, can be derived:

$$\begin{aligned} \mu_{eff}(\phi, k, pH, Ca^{2+}, VES) = & \frac{\mu_0}{12} \left(9 + \frac{3}{n}\right)^n (150k\phi)^{\frac{1-n}{2}} \\ & \times \left(1 + \frac{\mu_{\max}(pH, Ca^{2+}, VES)}{\mu_0} \exp\left(-0.5 \left(\frac{C_{VES} - C_{m,VES}}{W_1}\right)^2\right)\right) \\ & \times \exp\left(-\left(\frac{C_{Ca^{2+}} - C_{m,Ca^{2+}}}{W_2}\right)^2\right) \times \frac{(erf(bpH - c) + 1)}{W_3} \end{aligned} \quad (2.21)$$

2.3. Porescale parameters

2.3.1. Porosity

In reactive flow the solid species dissolves into liquid species, leading to a change in pore volume and thus a change in porosity. In this section the concept of reactive and fluid porosity is described.

The classic porosity, which represents the volume occupied by fluids, is considered the fluid porosity. The part of the rock that is reactive and thus can dissolve into the fluid phase, is called reactive porosity. Fluid porosity and reactive porosity combined give the total porosity of the grid cell. For non-reactive systems porosity is only depended on pressure changes due to compressibility of the rock, however in reactive flow the pore space also changes as a function of mineral (solid species) composition.

Bulk volume can be divided into three components, non-reactive volume, reactive volume and pore volume. Non-reactive volume does not dissolve, so it remains constant. Reactive volume is the part of the rock that reacts with the pore fluid and dissolves into the fluid phase. With these definitions the bulk volume and total porosity can be expressed as:

$$V_b = V_{nr} + V_r + V_\phi \quad (2.22)$$

$$\phi^T = \frac{V_r}{V_b} + \frac{V_\phi}{V_b} \quad (2.23)$$

$$\phi^T = \phi^r + \phi^p \quad (2.24)$$

Total porosity will always be constant, because when mineral is dissolving, reactive porosity will decrease but fluid porosity will increase by the same amount. Mineral saturation is defined as:

$$s_i^m = \frac{V_{ri}}{V_r + V_\phi} \quad (2.25)$$

Or, by substituting the definition of total porosity:

$$s_i^m = \frac{V_{ri}}{\phi^T V_b} \quad (2.26)$$

The equation for fluid porosity can be written as a function of total porosity and mineral saturation:

$$\phi = \phi_t \left(1 - \sum_{i=1}^{n_m} s_i \right) \quad (2.27)$$

Where n_m is the number of mineral species. In the case of only one reactive mineral, this equation becomes:

$$\phi = \phi_t (1 - s_s) \quad (2.28)$$

If the total porosity and the initial porosity of a layer are known, the mineral saturation can be calculated. Dissolution leads to change in mineral saturation and thus fluid porosity can be calculated in each time-step. [5]

2.3.2. Permeability

As matrix rock continues to dissolve and fluid porosity increases, other pore properties change as well. To update permeability the modified Kozeny-Carman model is used. [7]

$$k = k_0 \frac{\phi}{\phi_0} \left[\frac{\phi(1 - \phi_0)}{\phi_0(1 - \phi)} \right]^{2\beta} \quad (2.29)$$

Where β is an exponent determined from experimental data, if a value of 1 is assumed for β , this equation can be written as:

$$k = k_0 \left[\frac{(1 - \phi_0)^2}{(1 - \phi)^2} \right] \left(\frac{\phi}{\phi_0} \right)^3 \quad (2.30)$$

2.3.3. Pore structure

Pore radius is updated by:

$$r_p = r_{p0} \sqrt{\frac{k\phi_0}{k_0\phi}} \quad (2.31)$$

Interfacial area is updated by:

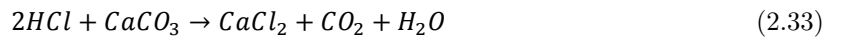
$$a_v = a_0 \frac{\phi r_{p0}}{\phi_0 r_p} \quad (2.32)$$

2.4. Reaction rate

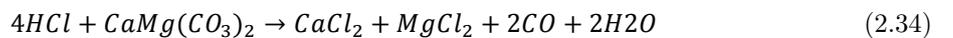
This section describes the reaction rate and the parameters that influence the reaction rate when introducing non-Newtonian, visco-elastic fluid.

When Hydrochloric acid (HCl) is introduced into a carbonate reservoir, different reactions can occur depending on the specific mineral content of the reservoir. The most common minerals found in carbonate reservoirs are calcium carbonate (calcite, $CaCO_3$), dolomite ($CaMg(CO_3)_2$) and Siderite ($FeCO_3$), which each have their own primary chemical reaction in acidizing:

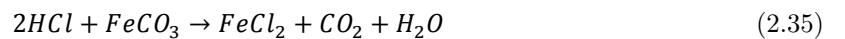
Calcite:



Dolomite:



Siderite:



In this work the reactive part of the reservoir is modeled to consist only of calcium carbonate, so only the first reaction is modeled. CaCl_2 is assumed to dissolve fully into the water:



In Newtonian flow physics it is sufficient to have a reaction rate that is only acid concentration dependent, because the flow of acid from the bulk fluid in the middle of the pore to the solid-fluid interface can be considered instantaneous because it is much faster than the surface reaction rate. With non-Newtonian fluids however, depending on the magnitude of the increase in viscosity, the flow rate of fresh acid to the solid-fluid interface will decrease and eventually will become slower than the reaction rate constant. At this point, the bottleneck in the reaction rate is the mass transfer. Acid propagation from the pore to the solid-fluid interface where it reacts, is displayed in figure 2.7.

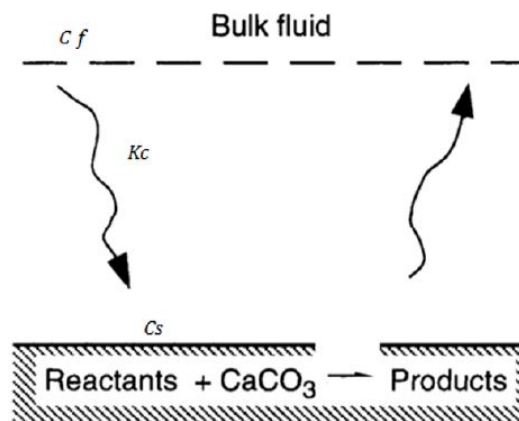


Figure 2.7: Acid propagation from the pore to the solid-fluid interface

To include this effect in the model, two parameters are needed: reaction rate constant (k_s) to express the rate of dissolution at the solid-liquid boundary, and the mass transfer coefficient (k_c) which describes the flow of fresh acid from the bulk fluid to the solid-liquid boundary.

Depending on the magnitude of the mass-transfer coefficient k_c , relative to the reaction rate constant k_s , 2 dissolution regimes can occur:

$k_c > k_s$: kinetically controlled regime: reaction at surface is slower than transport of acid from bulk fluid to rock/liquid interface.

$k_c < k_s$: mass transfer controlled regime: reaction at surface is faster than transport of acid from bulk fluid to rock/liquid interface.

The reaction rate constant is a fixed value for a given reaction. Because of this, the magnitude of the k_s/k_c -ratio is determined by the local mass-transfer coefficient which is a function of the pore geometry and fluid properties, the reaction rate and the local flow regime [2]. Heterogeneity, dissolution and varying viscosity values cause this ratio to not be constant over the reservoir with space and time, leading to different reaction mechanisms in different parts of the reservoir.

The amount of acid transported from bulk fluid to the fluid-solid interface is the same as the amount that is getting consumed by the reaction. Thus it can be expressed as a flux balance between the consumed and transported acid:

$$R(c_s) = k_c (C_f - C_s) \quad (2.37)$$

Where C_f is the concentration injected and C_s is the concentration at the fluid-solid interface. $R(C_s)$ is the reaction rate [m^2/s]. For simplicity first order kinetics are assumed, although in reality the reaction may be highly non-linear and complex. The reaction rate can also be expressed as a function of reaction rate constant and acid concentration at the interface:

$$R(c_s) = k_s C_s \quad (2.38)$$

Equating both equations yields the following expression for C_s :

$$C_s = \frac{k_c}{k_c + k_s} * C_f \quad (2.39)$$

Which can then be substituted to give:

$$R(C_s) = \frac{k_s k_c}{k_c + k_s} * C_f \quad (2.40)$$

Note that k_s is a constant for the reaction, obtainable from literature. How to obtain k_c will be discussed in the next section.

2.5. Mass-transfer coefficient

The mass-transfer coefficient is used to quantify transport of acid species from the bulk fluid in the center of the pore to the fluid-solid interface. The mass-transfer coefficient determines the reaction regime so it plays an important role of describing the dissolution process. To obtain the mass-transfer coefficient, we first need to define the Sherwood number. The Sherwood number represents the ratio of convective mass transfer to the rate of diffusive mass transport. For flow inside a straight pore of arbitrary cross-section, a good approximation to the Sherwood number is:

$$Sh = \frac{2k_c r_p}{D_m} = Sh_\infty + 0.35 \left(\frac{d_h}{x} \right)^{0.5} Re_p^{1/2} Sc^{1/3} \quad (2.41)$$

Where k_c is the mass-transfer coefficient [m/s], r_p is the pore radius [m], D_m the molecular diffusivity coefficient [m^2/day], Sh_∞ is the asymptotic Sherwood number of the pore, d_h is the pore hydraulic diameter [m], x is the distance from pore inlet [m], and Sc is the dimensionless Schmidt number which is defined as the ratio of momentum diffusivity (kinematic viscosity) and mass diffusivity. [?]

Under the assumption that the length of a pore is typically a few pore diameters, the average mass-transfer coefficient can be obtained by integrating this expression over a pore length [2], giving:

$$Sh = Sh_\infty + b Re_p^{1/2} Sc^{1/3} \quad (2.42)$$

Where b is defined as:

$$b = \frac{0.7}{m^{1/2}} \quad (2.43)$$

m is the pore length to diameter ratio. The first term of the equation represents the diffusive contribution, while the second term in the equation represents the convective contribution. Asymptotic Sherwood number depends on pore geometry. An assumed value of 3.0 is used for this thesis. A value of 0.7 for b is used, as is done in [2]. A typical value for Schmidt number is 1000 for liquids. If these values are assumed, then the convective part of the Sherwood number reads:

$$b = 7 Re_p^{1/2} \quad (2.44)$$

Rewriting equation 2.41 for k_c , yields the following expression:

$$k_c = 0.5 \frac{D_m}{r_p} Sh_\infty = 1.5 \frac{D_m}{r_p} + 3.5 \frac{D_m}{r_p} Re^{1/2} \quad (2.45)$$

Reynolds number is a dimensionless number that signifies the ratio of the inertial forces and the viscous forces. It is used to predict if flow will be laminar or turbulent. Reynolds number is defined as:

$$Re = \frac{\rho_f d_{pore} \underline{u}}{\mu} \quad (2.46)$$

Where ρ_f is the fluid density, \underline{u} the Darcy velocity, d_{pore} the pore diameter and μ the dynamic viscosity. Substituting this into our equation for mass-transfer coefficient yields:

$$k_c = 1.5 \frac{D_m}{r_p} + 3.5 \frac{D_m \rho_f^{1/2} d_p^{1/2} \underline{u}^{1/2}}{r_p \mu^{1/2}} \quad (2.47)$$

Molecular diffusivity coefficient is given by Einstein-Stokes equation:

$$D_m = \frac{k_B T}{6\pi\mu_0 r_{particle}} \quad (2.48)$$

Where k_B is the Boltzmann constant [$m^2 k g s^{-2} K^{-1}$] and $r_{particle}$ is the radius of the diffusing particle [m], μ_0 is the viscosity of the fluid without the particles. For simplicity it is assumed that $\mu_0 = \mu$. Substituting this into our equation for mass-transfer coefficient yields:

$$k_c = \frac{k_B T}{4\pi\mu r_p r_{particle}} + \frac{3.5 k_B T \rho_f^{1/2} d_p^{1/2} \underline{u}^{1/2}}{6 \pi \mu^{3/2} r_p r_{particle}} \quad (2.49)$$

Which can be rewritten by grouping constants, as:

$$k_c = \frac{k_B T}{4\pi r_{particle}} \frac{1}{\mu r_p} + \frac{3.5 k_B T}{6\pi r_{particle}} \frac{\rho_f^{1/2} d_p^{1/2} \underline{u}^{1/2}}{\mu^{3/2} r_p} \quad (2.50)$$

3

Numerical model

This chapter covers the numerical implementation of the governing equation and viscosity model described in chapter 2. The model is programmed within the Delft Advanced Research Terra Simulator (DARTS) simulation framework, developed at the Civil Engineering and Geoscience (CEG) Department at the Civil Engineering faculty of TU Delft. This simulation framework uses a new approach called Operator-Based Linearization (OBL) to discretize the physics. In the first section, the OBL-principle will briefly be explained. The second section discusses the needed simplifications to the viscosity expression to use it in the DARTS-framework. The third section gives the formulations of the operators.

3.1. Operator-Based Linearization

Operator-based linearization is a new approach for the fully implicit linearization of governing equations that describe flow and transport in porous media, proposed by D.V. Voskov [10]. It is based on an approximate representation of the physics, in a similar way as space and time are discretized in conventional simulations. The governing equations are written as a combination of two types of operators. The first are operators that contain spatially-altered parameters such as mesh geometry, porosity and permeability, the second are operators that depend on the system's thermodynamic state, such as pressure, temperature and chemical composition. During the simulation the operator values are linearly interpolated on a physics mesh of chosen accuracy.

3.2. Viscosity treatment

The expression for viscosity, equation 2.21, used for this model contains both spatially-dependent and state-dependent parameters, in such a way that it can not be rewritten as a multiplication of spatially-dependent (ξ) and state-dependent (ω) parameters. As such, a simplification of either the reservoir or the equation needs to be made. Because the viscosity is heavily dependent on the chemical composition of the fluid, the choice has been made to simplify the reservoir.

Simulations are run on a 2D structured grid. To make the viscosity equation work within the DARTS-framework, geological layers with different properties will be represented as horizontal layers with homogeneous spatial properties. So we will have a layer-cake model where each horizontal layer has constant spatially-dependent variables. With this, the viscosity equation per layer can be written as only constants and state-dependent variables. Keeping the initial porosity and total porosity for a horizontal layer constant, the change in porosity and permeability resulting from the chemical reaction between the acid and the rock matrix can be modeled as a function of only state-dependent parameters: fluid porosity will be a function of only solid composition, which means its only state-dependent.

Due to disappointing initial simulation results that will be shown and discussed in the results and discussion section, several simplifications have been made to the viscosity model. In real-world physics, presence of Ca^{2+} -ions initiate the viscosifying process. In the simulated model this dependency has been removed entirely as a way to reduce the amount of variables, to improve the numerical stability of the simulator. Also for this reason the shear thinning effect has been removed because this leads to too much rapid changes in the viscosity to simulate efficiently. The applied model only has a dependency on the pH-value and concentration of surfactant.

3.2.1. Reaction rate

The physical description of the reaction rate obtained from literature research is a highly complex pore scale model. Our purpose is to create a simulator on near-wellbore scale, so instead of simulating these pore-scale phenomena, approximations will be made. In this section our main model, and two simplifications for k_c will be discussed. As described in section 2.4, reaction rate is according to the equation:

$$R(C_s) = \frac{k_s k_c}{k_c + k_s} * C_f \quad (3.1)$$

To get a value for $R(C_s)$, the equation for the mass-transfer-coefficient (eq 3.3) that has been derived in section 2.5 needs to be filled in. Constants can be obtained from literature values and reservoir data. Pore radius and pore diameter is estimated and kept constant for simplicity in early stages of simulation. Due to numerical errors in the simulation, further simplifications have been made by keeping fluid density constant as well. In future work this must be a function of pressure, compressibility and mineral mole fractions. The pore radius and pore diameter have been written as a function of porosity, but have so far not been used.

Filling in the following parameters:

$$\begin{aligned} k_B &= 1.38064852e-23 \text{ m}^2 \text{ kg s}^{-2} \text{ K}^{-1} \\ T &= 318 \text{ K} \\ \rho_f &= 1000 \text{ [kg/m}^3\text{]} \\ r_{particle} &= 1.2 \times 10^{-10} \text{ m} \\ r_p &= 10^{-5} \text{ m (estimated)} \\ d_{pore} &= 2 \times 10^{-5} \text{ m (estimated)} \end{aligned}$$

Into the expression for mass-transfer coefficient:

$$k_c = \frac{k_B T}{4\pi\mu r_p r_{particle}} + \frac{3.5 k_B T \rho_f^{1/2} d_p^{1/2} u^{1/2}}{6 \pi \mu^{3/2} r_p r_{particle}} \quad (3.2)$$

Which can be rewritten by grouping constants, as:

$$k_c = \frac{k_B T}{4\pi r_{particle}} \frac{1}{\mu r_p} + \frac{3.5 k_B T}{6\pi r_{particle}} \frac{\rho_f^{1/2} d_p^{1/2} u^{1/2}}{\mu^{3/2} r_p} \quad (3.3)$$

Yields the following equation:

$$k_c = a * \frac{1}{\mu} + b * \frac{\rho^{1/2} u^{1/2}}{\mu^{3/2}} \quad (3.4)$$

Where a and b are the constants:

$$\begin{aligned} a &= 2.917975597310749 \times 10^{-7} \\ b &= 4.306142887336391 \times 10^{-10} \end{aligned}$$

In the results section it will be shown that this model had proven to be too complex to work for our purposes, so two simplifications of the real physics have been used. The first simplified model neglects the velocity-dependency but keeps the viscosity-dependency of the reaction rate:

$$k_c = \frac{a}{\mu} + \frac{b}{\mu^{3/2}} \quad (3.5)$$

Simplified model two sets a constant k_c , resulting in a constant reaction rate.

3.2.2. Molar composition to weight percent conversion

DARTS is a compositional simulator, so it uses chemical composition of components in its simulations. The viscosity model that is applied here uses weight percentage to specify concentration. To determine the viscosity with this model, a conversion has to be made between mass percentage and molar composition. The equation used for this can be derived from the following equations.

$$w_c = \frac{wt\%_c}{100} = \frac{m_c}{m_{total}} \Rightarrow m_c = w_c \cdot m_{total} \quad (3.6)$$

$$m_c = n_c \cdot MW_c \Rightarrow n_c = \frac{m_c}{MW_c} = \frac{x_c \cdot m_{total}}{MW_c} \quad (3.7)$$

These two equations lead to the equation implemented for the conversion:

$$x_c = \frac{n_c}{n_{total}} = \frac{w_c/M_c}{\sum w_j/M_j} \quad (3.8)$$

3.3. Operators

The governing equation is written in operator form so that it can be used in the DARTS-framework. To define the operators used, the mass-balance equation needs to be discretized. A wo-Point Flux Approximation (TPFA) is used with upstream weighting and a backward Euler approximation in time. Capillarity and gravity are neglected. The finite-volume fully implicit discretization of the mass balance equation reads:

$$V \left(\left(\phi \sum_{j=1}^{N_f} x_{cj} \rho_j s_j \right)^{n+1} - \left(\phi \sum_{j=1}^{N_f} x_{cj} \rho_j s_j \right)^n \right) - \Delta t \sum_{l \in L} \left(\sum_j^{N_f} x_{cj}^l \rho_j^l T_j^l \Delta p^l \right) - V \Delta t \sum_{k=1}^{N_k} v_{ck} r_k = 0 \quad (3.9)$$

In case of one-phase flow, the discretized conservation of species equation for component c reads:

$$V \left((\phi x_c \rho_f s)^{n+1} - (\phi x_c \rho_f s)^n \right) - \Delta t \sum_{l \in L} (x_c^l \rho_f^l T_l \Delta p^l) - V (\Delta t v_c r) = 0 \quad (3.10)$$

Where V is the volume of a control volume, The flux is summed over all interfaces L between the control volume and other grid blocks. T is the transmissibility. The porosity can be split up into a product of the spatially distributed initial porosity, and a state-dependent expression, using the equation for compressibility that relates the change of porosity to the change in pressure:

$$\phi = \phi_0 (1 + c_r (p - p_{ref})) \quad (3.11)$$

The operator form is defined as:

$$a(\xi) (\alpha_c(\omega) - \alpha_c(\omega_n)) + \sum_t b(\xi, \omega) \beta_c(\omega) - c(\xi) \gamma_c(\omega) = 0 \quad (3.12)$$

Where operators a , b and c contain spatially dependent variables (ξ), and operators α , β and γ contain state-dependent variables (ω). ω indicates a state-dependent parameter and ξ indicates a spatially-dependent parameter. $\alpha(\omega_n)$ signifies the current time-step and $\alpha(\omega)$ signifies the previous time-step.

The parameters can be described as either functions of spatial coordinate ξ or physical state ω . State-dependent, and both state- and spatially-dependent parameters are:

- $\phi(\xi, \omega)$: porosity
- $k(\xi, \omega)$: permeability
- $\mu(\xi, \omega)$: viscosity
- $r_k(\xi, \omega)$: reaction rate
- $x_c(\omega)$: mole fraction of component c
- $P(\omega)$: pressure
- $s(\omega)$: fluid saturation
- $\rho_f(\omega)$: fluid molar density
- $u(\xi, \omega)$: fluid velocity

If we assume constant total porosity, initial porosity and initial permeability over each horizontal layer, the porosity, permeability and viscosity terms simplify to being only state (ω)-dependent in the specific layer. The operators are given by the following expressions: Spatially altered operators:

$$a(\xi) = \phi_0(\xi)V(\xi) \quad (3.13)$$

$$b(\xi, \omega) = \Delta t \Gamma^l(\xi) (p - p^l) \quad (3.14)$$

$$c(\xi) = \Delta t V(\xi) \quad (3.15)$$

State-dependent operators are:

$$\alpha_c(\omega) = (1 + c_r (p - p_{ref})) x_c \rho_f S \quad (3.16)$$

$$\beta_c(\omega) = x_c^l \rho_f^l \frac{k^l}{\mu_l} \quad (3.17)$$

$$\gamma_c(\omega) = v_c r \quad (3.18)$$

4

Results

This chapter shows and discusses the results obtained from the simulation. The first sections show the functionality of the model itself, first in 1D, then in 2D. Results of the full model are shown in section the main viscosity model results, as well as results after applying the various simplifications that were mentioned in chapter 3. Motivation for further simplifications will be given and elaborated on.

4.1. Results and discussion 1D

To test if the simulation is working properly, the model has first been made in 1D. Plot results of non-reactive-, and reactive flow are shown in figure 4.1 and figure 4.1, respectively. table 4.1 shows the injection and reservoir conditions. Other simulation parameter are arbitrary, as this graph is just for .

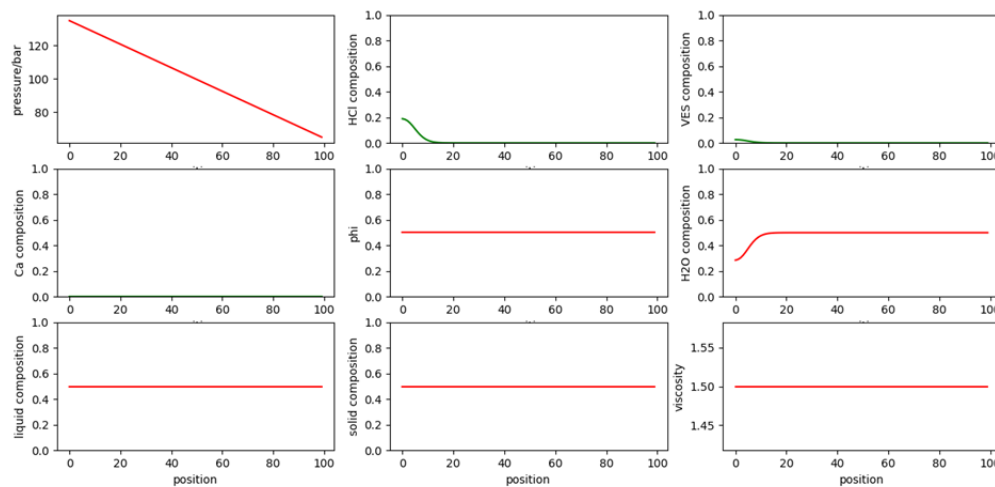


Figure 4.1: 1D non-reactive simulation results.

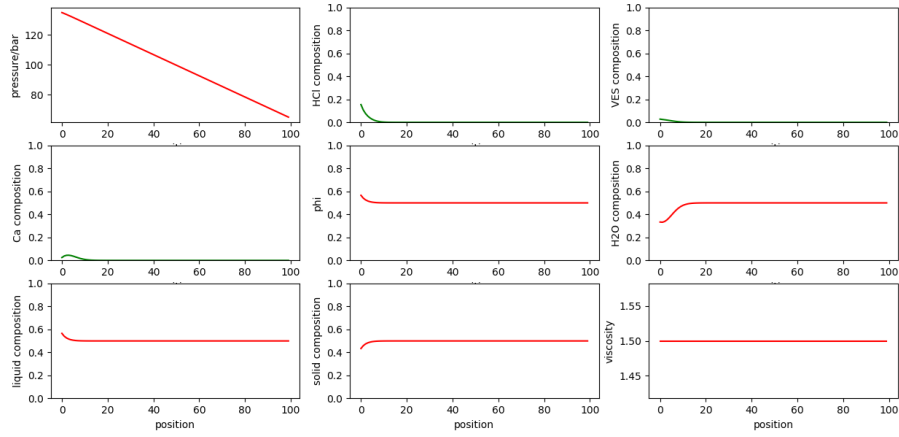


Figure 4.2: 1D reactive simulation results.

	H^+	VES	CA^{2+}	CO_2	H_2O	$CaCO_3$
Injection conditions 1D	0.3803	0.0522	1e-8	1e-8	0.5675	n/a
Initial conditions 1D	1e-8	1e-8	1e-8	1e-8	0.5	0.5

Table 4.1: 1D 6-component simulation injection and initial conditions

These plots have been made to confirm that 1D reactive and non-reactive 6-component flow is working appropriately. Note that injection conditions have been scaled to the reservoir, as the reactive rock formation is part of the composition. Pressure drop across the reservoir, flow and reaction rate is as expected.

4.2. Initial results 2D

This section shows initial simulation results. figures 4.3 and 4.4 show results for 2D reactive flow with constant reaction rate, in homogeneous and heterogeneous reservoir, respectively. Figure 4.3 shows results for three different types of viscosity. The first row shows propagation with constant viscosity, second row shows propagation with state-dependent viscosity, third row shows propagation with state- and shear dependent viscosity.

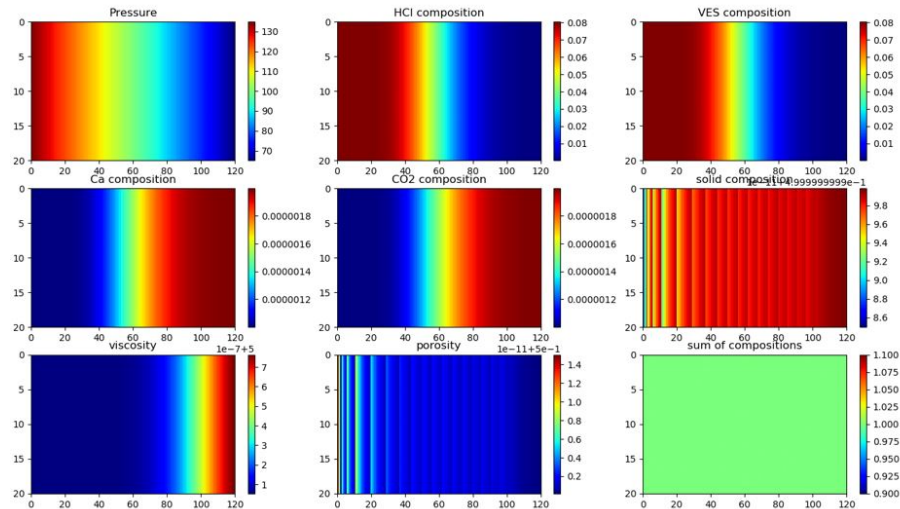


Figure 4.3: 2D simulation results for homogeneous reservoir with constant viscosity and constant reaction rate.

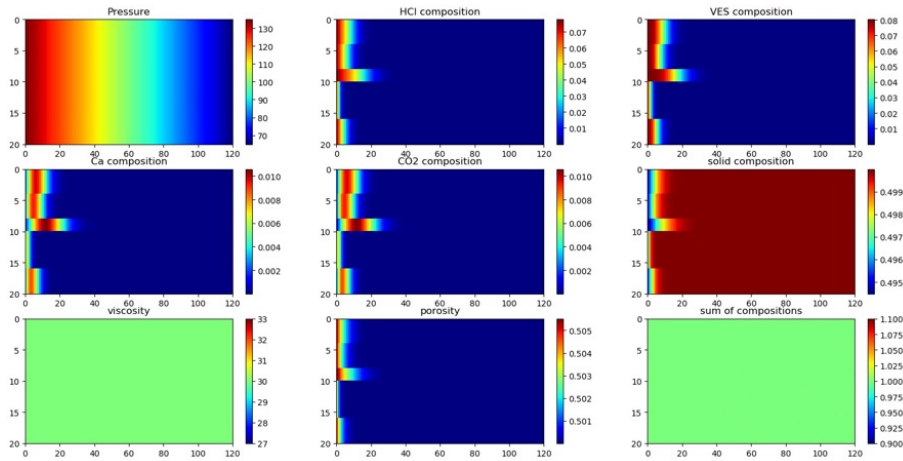


Figure 4.4: 2D simulation results for heterogeneous reservoir with constant viscosity and constant reaction rate.

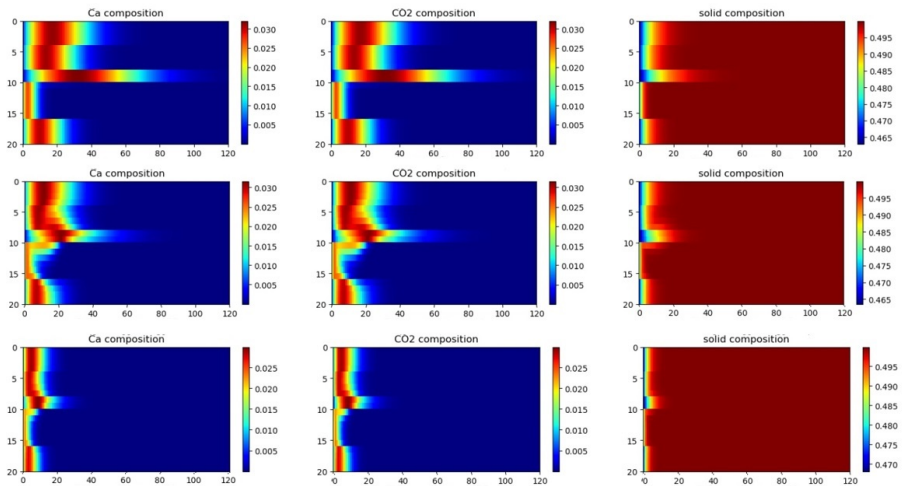


Figure 4.5: 2D simulation results for viscosity variations. First row is results for constant viscosity. Second row is results for state-dependent viscosity. Third row is results for state- and shear-dependent viscosity.

What we can conclude from these plots is that 6-component flow and constant reaction rate is working as expected. No diversion can yet be observed, only an overall increase of viscosity over all the injected fluid, leading to a reduction in flow velocity.

4.3. Results full-complexity 2D model

Figures 4.6 and 4.7 show the simulation results for the full model, as described in the physics section, without further simplifications.

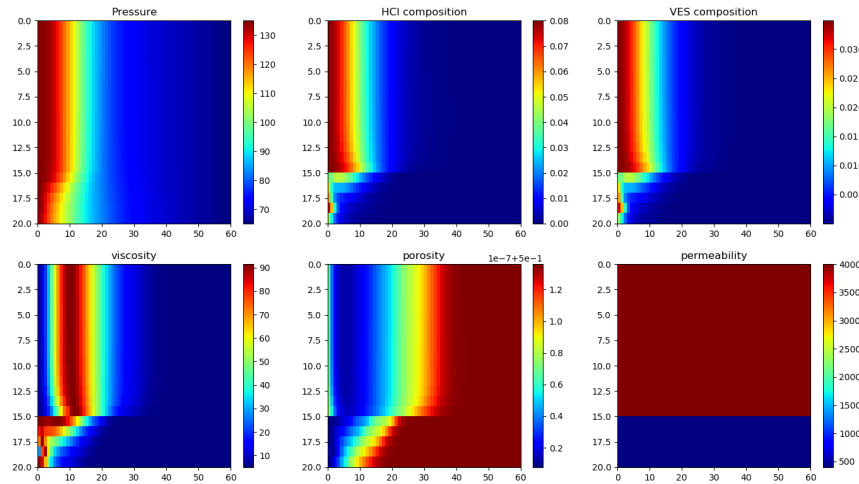


Figure 4.6: 2D simulation results for full viscosity model, as described in Physics section.

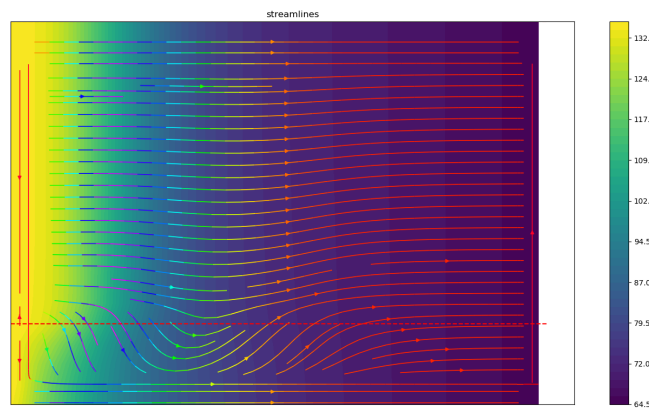


Figure 4.7: 2D flow lines results for full viscosity model, as described in Physics section.

The full-complexity model shows barely any signs of diversion. Further increases of parameters such as reaction rate induce numerical instability, which will be discussed in the next section. Because of the diversion not functioning in its current state, it was decided to simplify the model. The assumption has been made that Ca^{2+} -ions are freely available through-out the reservoir. This does not describe the real-world physics accurately because where reaction has occurred Ca^{2+} -concentration will be significantly higher. However, it is a reasonable assumption to be made because at any time when the injected fluid is inside the carbonate reservoir, there will be a reaction occurring at the solid/liquid-interface, and the brine inside the reservoir is likely to have some calcium-ions inside, possibly from pressure-solution of $CaCO_3$. Furthermore the dependency on acid concentration and VES concentration have been made linear. The acid concentration is not a very realistic simplification as in the real-world physics the viscosity shoots up drastically when all acid is spent, but it is a necessary one to improve stability of the simulator. In future research the instability should be resolved, and the original exponential relation can be used.

4.4. Results simplified 2D model

Figures 4.8 and 4.9 show the results and flow lines for the simulation with linear increase in viscosity and constant reaction rate dependent on acid concentration.

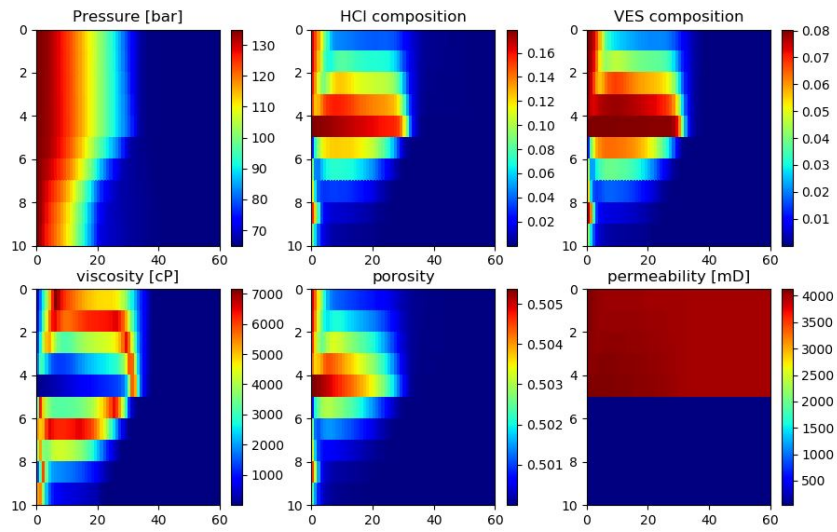


Figure 4.8: 2D simulation results for simplified viscosity model for pressure, acid and surfactant compositions, viscosity, porosity and permeability

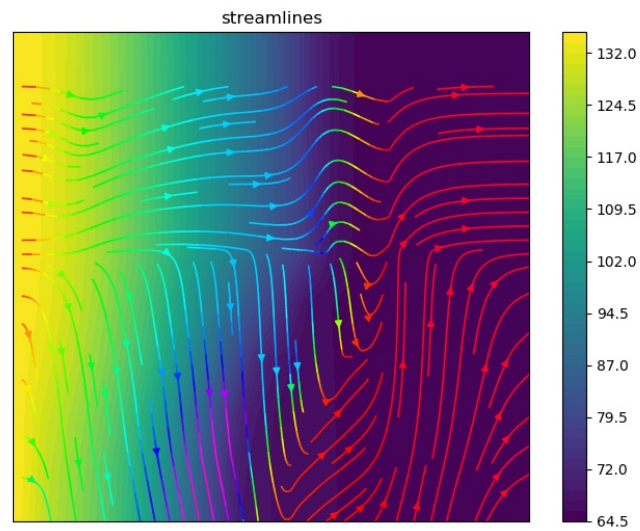


Figure 4.9: 2D simulation flow lines for simplified viscosity model.

Fresh acid and visco-elastic surfactant seem to accumulate in the bottom part of the upper (high-permeability) layer, creating a low viscosity pathway for most of that layer, which is not the desired effect of the simulation. Looking at the flowlines, it seems that flow gets diverted around the tip of the wormhole in the bottom of the upper layer. Being able to run the simulation for a longer time and with a faster reaction-rate is desired to see how the model would progress and react, however due to numerical instabilities this was not possible.

4.4.1. Numerical instabilities

The exact reason why the code is unstable has not been discovered, numerous runs of the simulation suggest that numerical instability occurs depending on the combination of values for viscosity, run time, and to a lesser extent reaction rate. The following cases cause instability in the model:

- Step changes in viscosity.
The viscosity expression is a base viscosity value plus a multiplication of the maximum attainable viscosity and a multiplier value between 0 and 1 which depends on the concentrations. If the multiplication factor's dependency on acid concentration is defined as a linear dependency, it will yield the best results numerically. With a quadratic dependency the code would crash after a run time of 5 days, whereas with a linear dependency code will be for 40 days run time. However if with the same value range of between 0 and 1, the dependency is quadratic or of high exponent, the code will be unstable after a run time of 3 days.
- Reaction rate too high.
If the reaction rate is too high, the code becomes unstable. This is not caused by acid or rock not being present in the cell, as a warning and correction has been coded to warn and correct the reaction rate if solid composition were to fall below zero, which did not occur yet. The problem could potentially be caused by the change in porosity as a result of the change in solid composition, though this will have to be looked into in future research.
- Run time too long or max time-step too high.
If the code is run for too long, the code crashes without any indications of outliers in viscosity, reaction rate, compositions, porosity or permeability. Increasing the max time-step too much will also cause the code to become unstable for numerical reasons.

4.5. Sensitivity analysis

A meaningful sensitivity analysis can not be made at the current state of the simulator due to the code crashing at different times, depending on the combination of viscosity expression, reaction rate and run time. If parameters are increased or decreased by too much the code will become unstable and a working combination of before-mentioned parameters has to be found by trial-and-error. Individual parameter sensitivity will be given for the acid and VES compositions. The focus of this section is on analysing the sensitivity of the diversion process and flow lines, to variation in simulation conditions. Simulation parameters have been kept similar on each sensitivity analysis run, but this was not always possible. On the low viscosity increase runs the run time had to be shortened to ensure stability. If the viscosity increase due to the viscosifying mechanism is multiplied by a scalar, the propagation of injected fluid decreases all over the reservoir, and run time had to be drastically increased to be able to make a visual comparison of the plot results.

Sensitivity to the main composition parameters has been given in section 2.2.1. However due to stability issues the linear viscosity model has been used.

Sensitivity to acid and VES composition for the multiplication factor for the simplified model is shown in figure 4.10. The quadratic relation however is very unstable.

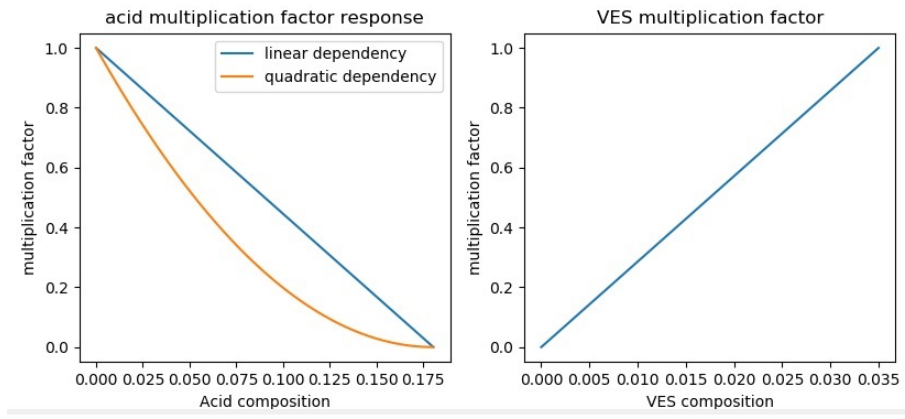


Figure 4.10: Sensitivity of multiplication factor to acid and VES composition.

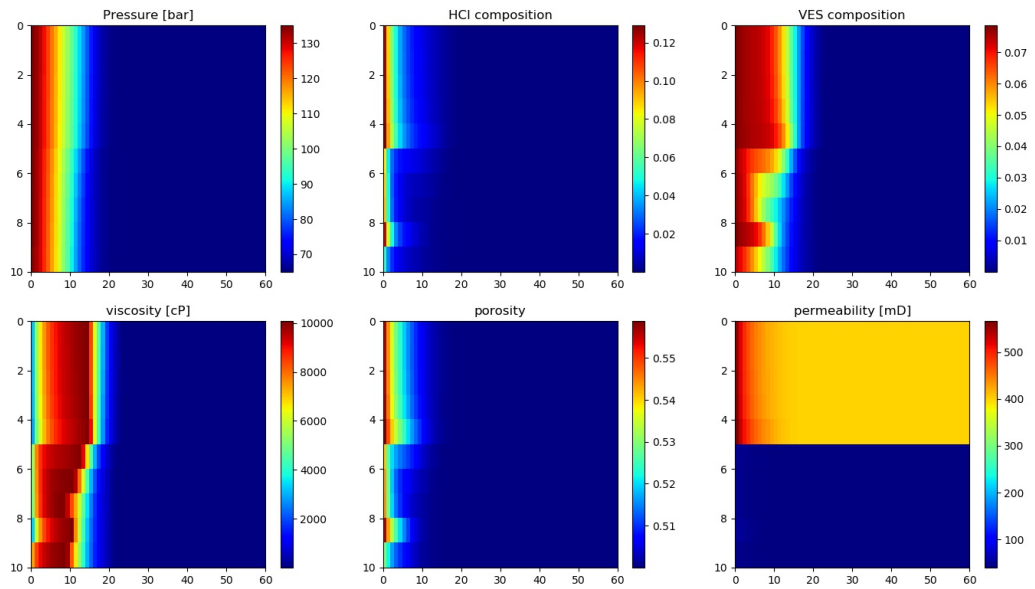


Figure 4.11: plot results for $k_{upperlayer} = 400mD$, run time = 1000d, $dt = 5d$, $\mu_{max} = 10500cP$

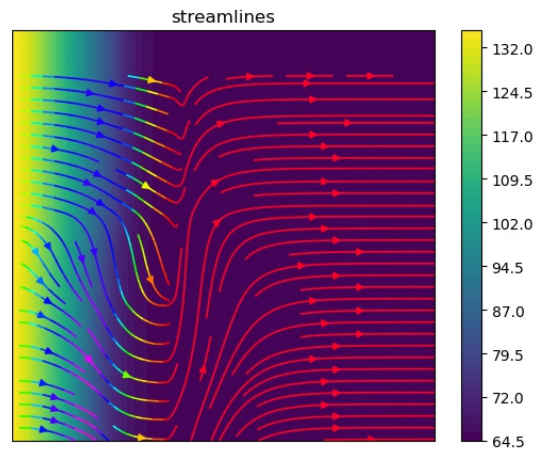


Figure 4.12: flowlines for $k_{upperlayer} = 400mD$, run time = $1000d$, $dt = 5d$, $\mu_{max} = 10500cP$

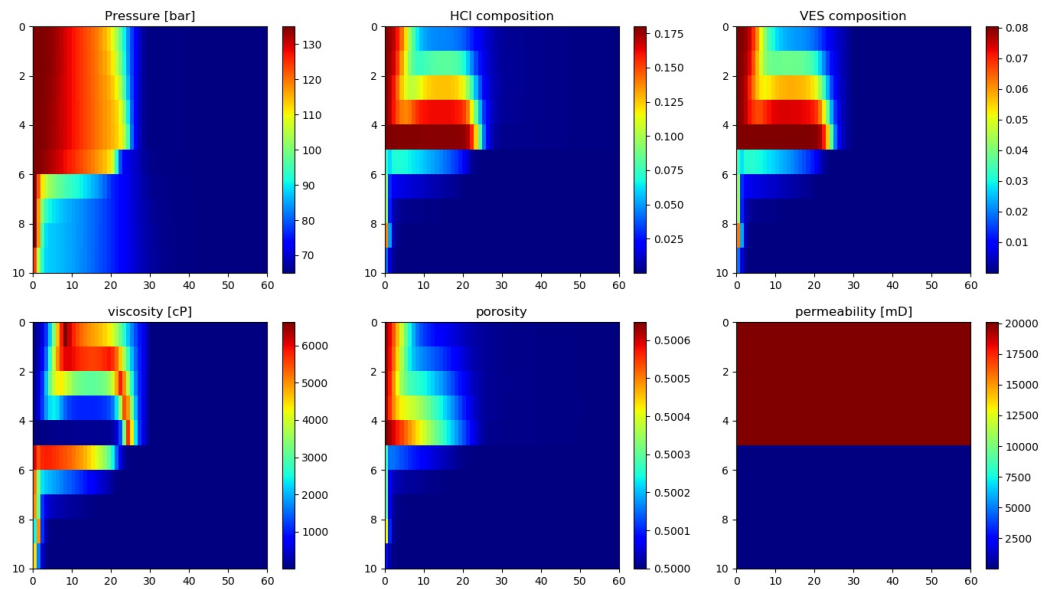


Figure 4.13: plot results for $k_{upperlayer} = 20000mD$, run time = $10d$, $dt = 0.2d$, $\mu_{max} = 10500cP$

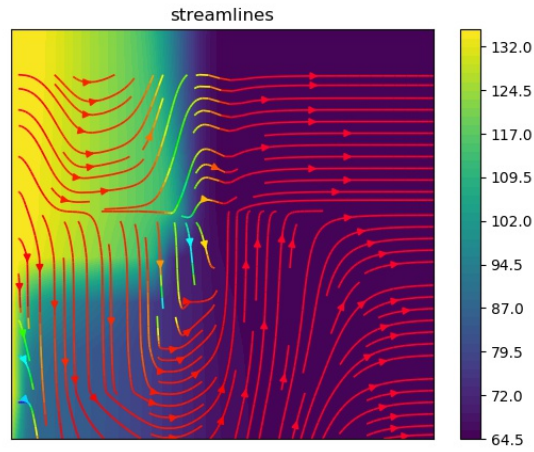


Figure 4.14: flowlines for $k_{upperlayer} = 20000mD$, run time = $10d$, $dt = 0.2d$, $\mu_{max} = 10500cP$

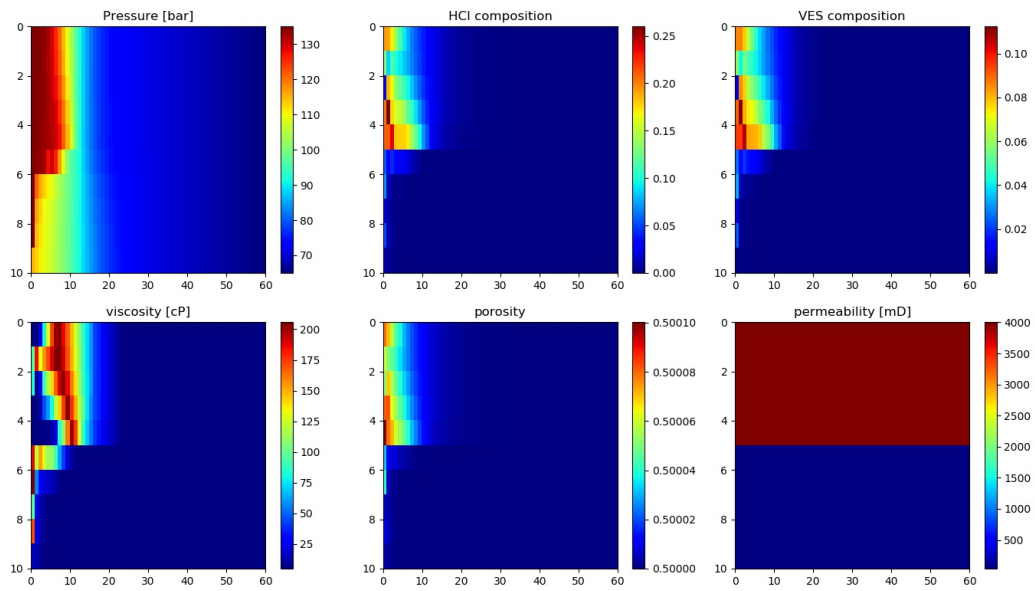


Figure 4.15: plot results for $k_{upperlayer} = 4000mD$, run time = $1.7d$, $dt = 0.2d$, $\mu_{max} = 350cP$

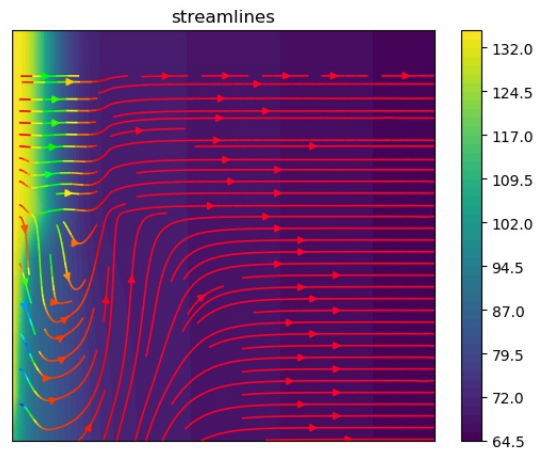


Figure 4.16: flowlines for $k_{upperlayer} = 4000mD$, run time = $1.7d$, $dt = 0.2d$, $\mu_{max} = 350cP$

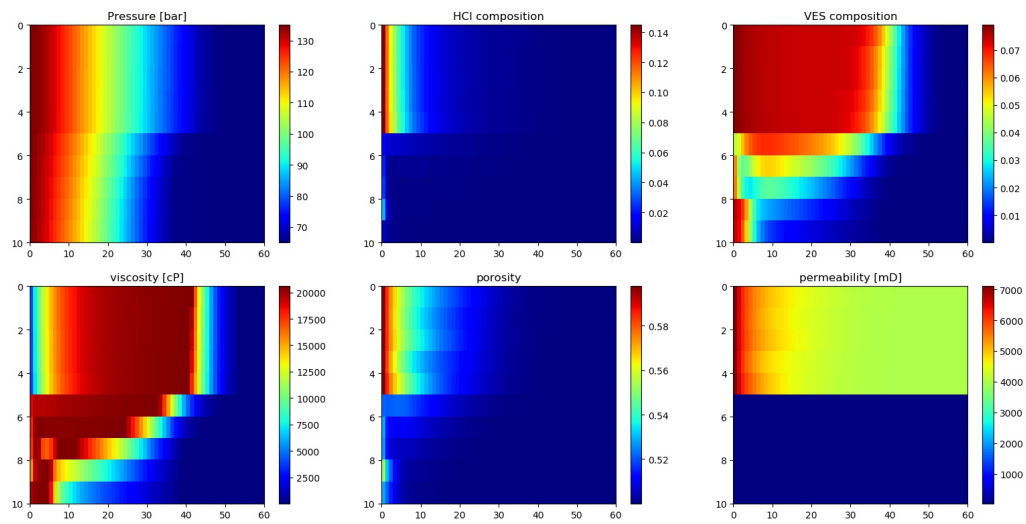


Figure 4.17: plot results for $k_{upperlayer} = 4000mD$, run time = $1500d$, $dt = 5d$, $\mu_{max} = 21000cP$

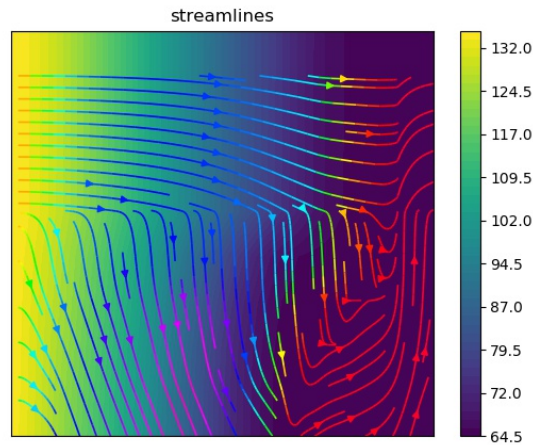


Figure 4.18: flowlines for $k_{upperlayer} = 4000mD$, run time = 1500d, dt = 5d, $\mu_{max} = 21000cP$

	fig 4.8, 4.9	fig 4.11, 4.12	fig 4.13, 4.14	fig 4.15, 4.16	figure 4.17, 4.18
nx [-]	60	60	60	60	60
ny [-]	10	10	10	10	10
Xr [-]	1	1	1	1	1
T [K]	318	318	318	318	318
$k_{i,upper}$ [mD]	4000	400	20000	4000	4000
$k_{i,lower}$ [mD]	40 k	40	40	40	40
thickness _{upper} [m]	5	5	5	5	5
thickness _{lower} [m]	5	5	5	5	5
dt _{max} [d]	1	5	0.2	0.2	5
run time [d]	60	1000	10	1.7	1500
μ_{max} [cP]	10500	10500	10500	350	21000
Reaction rate	constant, x_c -dependent rate	constant, x_c -dependent	constant, x_c -dependent	constant, x_c -dependent	constant, x_c -dependent

Table 4.2: Simulation parameters for results and sensitivity analysis

Table 4.2 shows an overview of the simulation parameters used for the results and sensitivity analysis.

Figures 4.11 to 4.14 compare the results for a decreased and increased initial permeability of the upper layer. Figure 4.11 with $k_{i,upper} = 400mD$ shows a more homogeneous propagation of injected fluids compared to figure 4.13, due to the permeability of the two layers having only a factor 10 difference instead of a factor 500. Figure 4.11 does seem to have a start of a wormhole in the lower layer, although propagation is still the deepest in the high permeability layer. Due to numerical instability this can not be ran for a longer time to investigate how this will develop. Figure 4.13 with a higher initial permeability for the upper layer seems to divert flow to the lower part of the upper layer. similarly to the original results from figure 4.8.

Figures 4.15 to 4.18 compare the results for a decreased and increased maximum viscosity. Figure 4.15 shows a similar pattern in viscosity as fig 4.8 in the results section. The plot penetrates less deep into the reservoir due to the drastically decreased run time which is necessary to keep the code stable. Based on this result it is reasonable to assume that lowering the maximum viscosity from 10500 cP to 350 cP does not affect the diversion process. Figure 4.17 shows the results for increasing the maximum viscosity to 21000 cP. This slowed down the overall propagation of injected fluid drastically, making it difficult to compare it with the main results. Dissolution is only occurring uniformly near the injection well.

4.6. Conclusion and recommendations

What can firstly be concluded is that the process of diversion of acid with self-diverted acid systems is very complex and difficult to model. Besides the complexity of the physics, unexpected numerical instability issues impede further analysis of the results and thus further improvements of the model. However, some preliminary conclusions can be made based on the results from the current state of the simulator. From the results with a simplified viscosity and reaction rate it can be concluded that application of the simplified model affects flow patterns and creates barriers to flow along which injected fluid is diverted, although simulation of the desired effect of diverting flow to low-permeability zone has not been achieved. From the current results it seems that big permeability difference are needed to observe the effects of diversion in the composition values. With a factor 10 permeability difference between layers the flow pattern resembles uniform dissolution, whereas a factor 100 difference shows wormhole formation.

For future continuation of this project it is very important to look into the cause for the numerical instability of the simulation. The first priority should be to find out why the simulator crashes when increase of viscosity value occurs more steeply. The biggest benefit of being able to vary the parameters more freely and run the code for a longer time is that it will improve analysis of the model, allowing for more certainty about if the diversion process is captured properly in the model. This is because of two reasons, firstly because porosity increase from dissolution can then be increased more, secondly because being able to increase run time would show us the behaviour of the model over a longer time period. When numerical stability has been accomplished, the full viscosity model can be reintroduced and analyse can be made to see if it behaves as expected.

Bibliography

- [1] Khalid S. Asiri et al. Stimulating naturally fractured carbonate reservoirs. 2013.
- [2] Panga et al. Two-scale continuum model for simulation of wormholes in carbonate acidization. *Chemical Engineering Science* 56, 56:4771–4786, 2001.
- [3] Skoog et al. Fundamentals of analytical chemistry. *Fundamentals of Analytical Chemistry* (9th ed.), pages 415–4161, 2013.
- [4] Yue Hong et al. Numerical simulation and field application of diverting acid acidizing in the lower cambrian longwangmiao fm gas reservoirs in the sichuan basin. *Production Engineering 2018 course*, Delft University of Technology, 2011.
- [5] Denis Voskov Keshav Kala. Element balance formulation in reactive compositional flow and transport with parameterization technique, 2018.
- [6] Mingli Liu. Diverting mechanism of viscoelastic surfactant-based self-diverting acid and its simulation. *Journal of Petroleum Science and Engineering*, 105:91–99, 2013.
- [7] Ping Liu. Analysis and simulation of rheological behavior and diverting mechanism of in situ self-diverting acid. *Journal of Petroleum Science and Engineering*, 132:39–52, 2015.
- [8] R. R. Ratnakar. Modeling, analysis and simulation of wormhole formation in carbonate rocks with in situ cross-linked acids. *Chemical Engineering Science*, 90:179199, 2013.
- [9] Schlumberger. Viscoelastic diverting acid. URL <https://www.slb.com/completions/stimulation/acidizing-services/vda-acid>.
- [10] D.V. Voskov. Operator-based linearization approach for modeling of multiphase multi-component flow in porous media. *Journal of Computational Physics*, 337:275–288, 2017.
- [11] P.L.J. Zitha. Matrix acidizing lecture slides. *Production Engineering 2018 course*, Delft University of Technology, 2011.
- [12] P.L.J. Zitha. Formation damage lecture slides. *Production Engineering 2018 course*, Delft University of Technology, 2011.